Appl. Phys. A (2016) 122:762
DOI 10.1007/s00339-016-0274-6

Applied Physics A
Materials Science & Processing

Bridged single-walled carbon nanotube-based atomic-scale mass sensors

H. R. Ali-Akbari[1] · M. Shaat[2] · A. Abdelkefi[2]

Received: 8 May 2016 / Accepted: 12 July 2016 / Published online: 26 July 2016

Abstract The potentials of carbon nanotubes (CNTs) as mechanical resonators for atomic-scale mass sensing are presented. To this aim, a nonlocal continuum-based model is proposed to study the dynamic behavior of bridged single-walled carbon nanotube-based mass nanosensors. The carbon nanotube (CNT) is considered as an elastic Euler–Bernoulli beam with von Kármán type geometric nonlinearity. Eringen's nonlocal elastic field theory is utilized to model the interatomic long-range interactions within the structure of the CNT. This developed model accounts for the arbitrary position of the deposited atomic-mass. The natural frequencies and associated mode shapes are determined based on an eigenvalue problem analysis. An atom of xenon (Xe) is first considered as a specific case where the results show that the natural frequencies and mode shapes of the CNT are strongly dependent on the location of the deposited Xe and the nonlocal parameter of the CNT. It is also indicated that the first vibrational mode is the most sensitive when the mass is deposited at the middle of a single-walled carbon nanotube. However, when deposited in other locations, it is demonstrated that the second or third vibrational modes may be more sensitive. To investigate the sensitivity of bridged single-walled CNTs as mass sensors, different noble gases are considered, namely Xe, argon (Ar), and helium (He). It is shown that the sensitivity of the single-walled CNT to the Ar and He gases is much lower than the Xe gas due to the significant decrease in their masses. The derived model and performed analysis are so needed for mass sensing applications and particularly when the detected mass is randomly deposited.

1 Introduction

Recently, the need for the production and use of nano-components and nano-devices has been significantly increased. These nano-systems are intensively needed for biological, medical, physical, and chemical purposes. A nano-device can reflect a property change to measure a certain physical quantity. To improve the sensitivity of these devices, highly sensitive small resonators are integrated. These resonators should be very small in size and should be made of special materials to enhance their abilities for measuring different physical quantities.

Nowadays, mechanical resonators are widely used in various micro-/nanoscale applications. The operating principle of a mechanical resonator is based upon a frequency shift due to the deposited physical quantity. Then, the value of the physical quantity which is proportional to the induced shift in the frequency of the resonator is estimated using a mathematical model. To achieve accurate predictions and high sensitivity, mechanical resonators with high quality factors and high frequencies are needed [1, 2, 3]. In addition, these nano-devices have to be integrated with accurate mathematical models to get precise measurements and estimations. For more illustration, mechanical resonators with high quality factors give very high amplitude of vibration at resonance, and hence, their resonant frequencies can be easily detected when compared to resonators with lower quality factors. In addition to that, resonators with high frequencies are more sensitive than

✉ A. Abdelkefi
abdu@nmsu.edu

[1] Sharif Technology Services Complex, Sharif University of Technology, Tehran, Iran

[2] Department of Mechanical and Aerospace Engineering, New Mexico State University, Las Cruces, NM 88003, USA

those of lower frequencies. In addition to the quality factor and the frequency, the accuracy of the measurements is highly affected by how much the used mathematical model fits with the real behavior of the resonator. To achieve precise measurements, accurate mathematical models should account for the resonators' size effects and the discrete nature of their material structures [4, 5–7].

Some attempts have been made to propose mechanical resonators with high quality factors and sensitivities. One attempt is to control the dimensions of the resonator along with the material type and their material structure contents [8, 9]. A quality factor up to 10,000 is obtained by fabricating 40-nm-thick resonators made of nanocrystalline materials with grain sizes within the range 10–100 nm [8, 9]. In a recent study, quality factors exceeding one million are achieved using a single-crystalline diamond nano-resonator [1]. Other trials have been performed in which the resonators were operated in special conditions, such as putting them in vacuum chambers and/or at cryogenic temperatures [3]. Although these attempts were successful, CNTs have shown unrivaled success when integrated in mass sensing applications. Lassagne et al. [10] reported that carbon nanotubes (CNTs) are promising candidates to fabricate ultra-sensitive mechanical resonators. For example, 1.4 zepto-gram resolution is achieved using 1-nm-diameter CNT [10]. The mass of a nanotube is very small (few attograms) and its mechanical stiffness is very high which result in very high resonant frequency for CNTs-based resonators [10]. Moreover, a 5 million quality factor is achieved with an ultra-clean CNT [3], a number that is not achieved using any other material so far.

Due to the intensive decrease in their sizes, mechanical resonators are made of nanomaterials, such as single-crystalline silicon/diamond, nano-crystalline silicon/diamond, or CNTs. In fact, the properties of nanomaterials are completely related to their material structure and their material size. The classical theories of materials science are not applicable for these materials because they lack the suitable length scales that can capture the size-dependent behavior of these types of materials. For instance, to model the mechanics of nanomaterials in micro-/nanoscale applications, the nonlocal features of their dispersive phonons should be counted in the developed model. Experimental investigations on materials composing a single crystal have shown that the dissociation energies and the interatomic potentials have nonlocal long-range contributions [11, 12, 13]. A CNT is a single-/multi-graphite layer(s) consisting of repeated unit cells, and each unit cell contains 1–4 graphite atoms depending on its structure type (chiral, zigzag, or armchair). Thus, CNTs exhibit acoustic and optical phonons with nonlocal features. Consequently, to accurately model CNTs, new measures should be introduced in the context of the mathematical model to reflect the nonlocal fields of dispersion phonons of CNTs. Recently, due to their ultra-high quality factors and resonant frequencies, their superior electronic properties, and their manufacturability, several studies were carried out to investigate the performance of CNTs as mass detectors [14, 15, 16, 10, 17], nano-sensors [15, 16, 18, 19, 20], and nanoresonators [21, 22, 23]. For example, Li and Zhu [24] proposed an optical weighing technique using a CNT. They were able to measure the mass of a single *Xe*-atom where a frequency shift of the CNT is observed due to the deposited atom. Chiu et al. [17] developed a clamped–clamped CNT-based nano-mechanical resonator as an atomic-scale mass sensor to measure the mass of *Xe* gas atoms. In their analysis, the atoms were assumed to be deposited at the middle point of the CNT-resonator because of its higher absorbability rather than other locations. In other efforts, the classical theories of continuum mechanics were used to model and/or characterize the mechanical behaviors of CNTs [25, 26, 27, 28, 29, 30]. As previously discussed, to accurately model CNTs in mass sensing applications, some measures should be introduced in the context of the continuum model to capture their material structure and size effects. This exceeds the limit of the applicability of the classical theories of continuum mechanics. In several recent researches [31, 32, 33, 34, 35, 36, 37], Eringen's nonlocal elastic field theory [38, 39] has been used to study the mechanical and dynamic characteristics of CNTs and CNT-based mass nano-sensors. Shen et al. [34] proposed a nonlocal-based Euler–Bernoulli beam model to study the sensitivity of double-walled CNTs and single-walled CNTs. They demonstrated that double-walled CNTs have less nano-mass detective sensitivity with respect to single-walled CNTs. Li et al. [37] developed a nonlocal Euler–Bernoulli beam model to determine the dynamic behavior of a single-walled carbon nanotube (SWCNT)-based mass sensors. In their analyses, the nanoscale mass is assumed to be landed at the middle span of the clamped–clamped CNT. However, depositing atomic-masses at a definite location on the nano-resonator's surface is not easy. Furthermore, it cannot be guaranteed that the atoms are kept attached to the same location all the time. This inspired us to propose a model which accounts the effects of the inertia and the arbitrary location of the deposited atomic-mass on the resonator's natural frequencies and its accuracy for mass detection.

In the present study, a nonlocal Euler–Bernoulli beam model is proposed to investigate the sensitivities of single-walled carbon nanotubes (SWCNTs) for the atomic-scale mass sensing applications. Eringen's nonlocal elasticity is utilized to capture the mechanics of CNTs in mass sensing applications. The applicability of the nonlocal theory for CNTs is discussed in Sect. 2. The geometric nonlinearity

of the CNT is included in the proposed model based on the von Kármán theory. Then, the derived nonlinear model is analytically solved to characterize the dynamic behaviors of bridged SWCNT-based mass sensors. In the context of this model, the arbitrary position of the atomic-scale mass is considered in the continuity equations of the beam where the atomic-mass can be deposited at any position along the beam's length. Through an eigenvalue problem analysis, the structural natural frequencies and associated mode shapes are analytically obtained. The developed model and the proposed analytical solutions are used to propose effective CNT-based mechanical resonator for atomic-scale mass sensing. The rest of this work is organized as follows: In Sect. 2, the concept of the nonlocal elasticity is discussed, showing the different nonlocal theories and the applicability for CNTs. Then, in Sect. 3.1, a CNT-based mechanical resonator for atomic-scale mass sensing is modeled based on the differential nonlocal elasticity. In Sect. 3.2, an eigenvalue problem analysis is carried out to determine the natural frequencies and associated mode shapes depending on the location of the atomic-mass. Sensitivity of a CNT-based sensor for various noble gas particles including Xe, Ar, and He is investigated in Sect. 4. Summary and conclusions are presented in Sect. 5.

2 Nonlocal elasticity review and applicability for CNTs

In the classical theories of continuum mechanics, the elastic body is modeled consisting of an infinite number of mass points that only account for the nearest neighbor interaction. However, the nonlocal interactions between the particles strongly affect the behavior of solids in micro-/-nanoscale applications [11, 12, 13]. In fact, in a continuum volume, each specific particle receives energies (or momentums) diffused by all of the other particles inside the continuum domain. Because of these diffused energies, the total momentum at a specific particle becomes the summation of the diffused momentums to the particle in addition to its local momentum. Eringen [38] showed the impacts of the nonlocal fields on different problems including electromagnetism, fluid dynamics, elasticity, and thermoelasticity. In the context of the nonlocal field theories, the elastic domain of application is modeled as an infinite number of points and each point receives energies diffused due to its long-range interactions with the other points in the domain. Because of these diffusion processes, the principle of thermodynamics does not hold at a local point, but it can be written only for the whole domain of application [40]. Consequently, in nonlocal domains, only the global balance laws should be applied [38]. On the other hand, in the case where the effects of nonlocality are trivial, the balance laws become local, and hence, the classical theories hold.

In the context of elasticity field problems, the strain (as a deformation measure) is introduced as the fundamental field. In linear theories of classical elasticity, the strain energy density at a certain point in the continuum is only a function of the local infinitesimal strain field at the considered point. However, Eringen proposed the nonlocal elasticity in which the strain energy density at a point depends on the local infinitesimal strain at the point of interest in addition to the strains of the neighboring points according to a weighted function (attenuation function) which depends on the in-between distances. This simple theory of nonlocal elasticity can be enhanced by modeling the material particle inside the elastic domain as a volume element accounting for the various forms of nonlocal residuals inside the material structure. This introduces the nonlocal micromorphic theory [38, 41]. Eringen's simple nonlocal elasticity can fit well with the acoustic branches of crystals [39]. However, the nonlocal micromorphic theory can fit with the various acoustic and optical branches of crystals [41].

According to Eringen's nonlocal elasticity theory, a stress field in an isotropic elastic continuum at a point $\boldsymbol{x}$ exists as a consequence of accumulating the imposed nonlocal strains of the neighboring points over the local strain field [39, 40] such that:

$$\sigma_{ij}(\boldsymbol{x}) = \Re\big(\lambda\varepsilon_{rr}(\boldsymbol{x})\delta_{ij} + 2\mu\varepsilon_{ij}(\boldsymbol{x})\big) \tag{1}$$

where $\Re(\blacksquare) = \int_{V \text{ or } V'} \alpha(|x - x'|)(\blacksquare)\mathrm{d}V'$ is an integral operator used to transform the local stress field, $\tau_{ij} = \lambda\varepsilon_{rr}(\boldsymbol{x})\delta_{ij} + 2\mu\varepsilon_{ij}(\boldsymbol{x})$, at a point $\boldsymbol{x}$ into a nonlocal stress field, $\sigma_{ij}(\boldsymbol{x})$. This integral operator depends on a kernel function which reflects the effects of the strain field of a neighbor point, $\boldsymbol{x}'$, on the local strain field of the reference point $\boldsymbol{x}$. λ and μ are the material Lame constants.

It should be mentioned that the attenuation function, $\alpha(|\boldsymbol{x} - \boldsymbol{x}'|)$, depends on an intrinsic material length scale parameter $e_0 a/l$ where a is a lattice parameter (granular distance), l is a macroscopic material length parameter (crack length, wavelength), and e_o is a constant appropriate to the material of the elastic body. The attenuation function, $\alpha(|\boldsymbol{x} - \boldsymbol{x}'|)$, is a positive scalar function which decays rapidly with increase in the distance $|\boldsymbol{x}' - \boldsymbol{x}|$. When a tends to zero, the attenuation function converts to a Dirac delta function where this function satisfies the normalization condition:

$$\int_{V'} \alpha(|\boldsymbol{x}' - \boldsymbol{x}|, \tau)\mathrm{d}V' = 1 \tag{2}$$

The infinitesimal strain measure in Eq. (1) is the conventional strain tensor which is given by:

$$\varepsilon_{ij}(\boldsymbol{x}) = \frac{1}{2}\left(u_{i,j}(\boldsymbol{x}) + u_{j,i}(\boldsymbol{x})\right) \tag{3}$$

where $u_i(\boldsymbol{x})$ is the displacement field of a material particle located at a point $\boldsymbol{x}$.

In the nonlocal linear elasticity problems, the stress field, σ_{ij}, is represented as a nonlocal field conjugate to the fundamental field which is the strain, ε_{ij}. Therefore, the equilibrium equation for a nonlocal elastic field can be written as follows:

$$\sigma_{ji,j}(x) + f_i(x) = \rho(x)\ddot{u}_i(x) \tag{4}$$

where $f_i(\boldsymbol{x})$ is the body force and $\rho(\boldsymbol{x})$ is the mass density. It should be noted that the nonlocal stress tensor is a symmetrical tensor. When compared to the local stress tensor, the nonlocal stress tensor has a wider bandwidth.

The total potential energy of a nonlocal elastic continuum occupying a volume V and bounded by a surface S can be obtained as follows:

$$\Pi = \int_V \int_{V'} \alpha(\boldsymbol{x}' - \boldsymbol{x})\left(\frac{1}{2}\lambda\varepsilon_{ii}(\boldsymbol{x}')\varepsilon_{jj}(\boldsymbol{x}) + \mu\varepsilon_{ij}(\boldsymbol{x}')\varepsilon_{ij}(\boldsymbol{x})\right)\mathrm{d}V'\mathrm{d}V - \int_V f_i u_i \mathrm{d}V - \int_S t_i u_i \mathrm{d}S \tag{5}$$

Equation (5) is formed such that the strain energy density at a point depends on the local infinitesimal strain in addition to the diffused fractions of the strains (depending on the attenuation function) at the neighbor points. In addition, the surface traction forces $t_i\mathrm{d}S$ and the body forces are considered having nonlocal features. The surface traction vector is related to the nonlocal stress tensor as follows:

$$t_i(\boldsymbol{x}) = \sigma_{ji}(\boldsymbol{x})n_j \tag{6}$$

where n_j is the surface normal vector.

Equation (4) demonstrates that Eringen's nonlocal theory is a modified classical theory of linear elasticity where the local stress field is replaced with a corresponding nonlocal stress field. Accordingly, Eringen's nonlocal elasticity can fit with the acoustic branches of CNTs. This forms the limit of the applicability of the theory for CNTs. To capture more nonlocal residuals, more advanced theories are needed such as nonlocal Micromorphic theory.

The necessity of applying the global balance laws forms the difficulty of applying the nonlocal theories to model the mechanics of continua in different applications [38]. Hence, solving the equilibrium equation, Eq. (4), for the local strain or displacement fields in its current form is challenging. Equation (4) is an integro-partial differential equation where it is very difficult to derive an analytical solution for the local fields [39]. This motivated Eringen [39] to introduce a differential operator as a replica for the integral one. This introduces the differential nonlocal elasticity. Eringen [39] derived the linear differential operator for a Green's function type attenuation kernel, $\alpha(\boldsymbol{x}' - \boldsymbol{x})$, having the following form:

$$\ell = (1 - (e_0 a)^2\nabla^2) \text{ i.e. } \ell\alpha(\boldsymbol{x}' - \boldsymbol{x}) = \delta(\boldsymbol{x}' - \boldsymbol{x}) \tag{7}$$

where ∇^2 is the Laplace operator and δ is the Dirac delta function. Hence, the nonlocal stress can be defined using the differential operator as:

$$\ell\sigma_{ji} = \tau_{ji} \tag{8}$$

Substituting Eq. (8) into Eq. (4) gives the equilibrium equation for a differential nonlocal elastic continuum as follows:

$$\tau_{ji,j} + \ell(f_i - \rho\ddot{u}_i) = 0 \tag{9}$$

It follows from Eq. (9) that a set of singular differential equations can be derived. These equations are easy to solve using the differential nonlocal elasticity. However, some difficulties still exist for applying the natural boundary conditions in the context of the differential nonlocal elasticity. According to Eqs. (5) and (6), the surface tractions should be considered accounting for its nonlocal characteristics. Solutions for the bending, vibration, and buckling behaviors of differential nonlocal beams were successfully derived accounting for the nonlocal natural boundary conditions [42, 43, 44, 45, 46, 47, and 48]. Lu et al. [46] derived the frequency equations and the mode shapes for simple supported, cantilever, and clamped–clamped Euler–Bernoulli differential nonlocal beams. Reddy [48] proposed analytical solutions for bending, vibration, and buckling of differential nonlocal simple supported beams. On the other hand, deriving solutions for differential nonlocal plates with natural boundary conditions is more complicated [49, 50]. This motivated Shaat [49] to propose an iterative procedure to solve nonlocal beams and plates where the local form of the boundary conditions can be used within the context of this iterative method.

3 CNT-based mass sensor modeling

3.1 System's modeling

One of the purposes in this study is to propose an accurate modeling of a CNT-based mechanical resonator for mass sensing applications. This developed model accounts for the nonlocal residuals inside the structure of the CNT and the geometric nonlinearity. The mechanical resonator is a clamped–clamped SWCNT with a length L and a diameter D, as shown in Fig. 1. The operating principle of this resonator is based on measuring the frequency shift due to

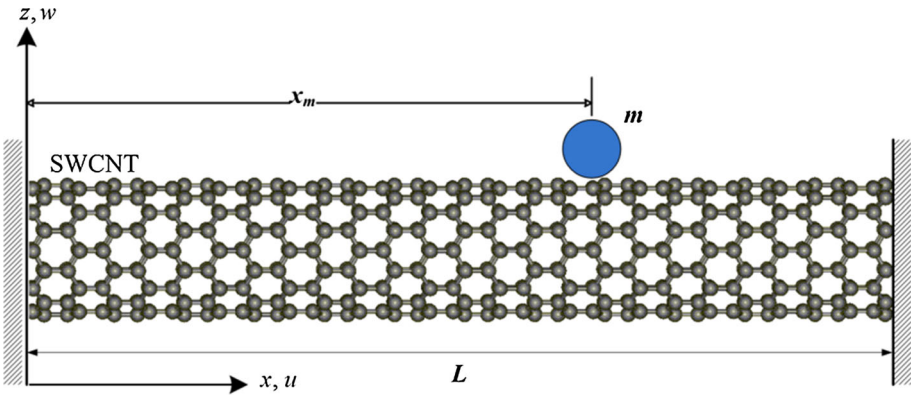

Fig. 1 Schematic representation of a bridged SWCNT-based atomic-scale mass sensor

the added mass and converting the frequency shift to an equivalent mass value. The mechanical resonator under consideration is designed to attract an atomic particle which can be deposited at any arbitrary location x_m along the resonator's free length, as shown in Fig. 1.

The considered SWCNT-based resonator is modeled according to Euler–Bernoulli beam theory with accounting for the interatomic long-range interaction via Eringen's nonlocal elasticity. The Hamilton's principle is utilized to derive the governing equations of motions and the corresponding boundary conditions of the bridged CNT.

The displacement fields as defined by Euler–Bernoulli beam theory are:

$$u_x(x,z) = u(x) - zw'(x); \quad u_y(x,z) = 0; \quad u_z(x) = w(x) \tag{10}$$

where u and w are the axial and the transverse displacements of a point that belongs to the axis of the CNT, respectively. The prime ($'$) represents the partial differentiation with respect to x.

To account for the geometric nonlinearity based on von Kármán theory, the beam (CNT) strain field can be defined as follows:

$$\varepsilon_{xx} = u' + \frac{1}{2}(w')^2 - zw'' \tag{11}$$

According to Eringen's differential nonlocal elasticity, the nonlocal stress is related to the local stress via a differential operator, as presented in Eqs. (7) and (8). Consequently, the nonlocal stress of the CNT-based resonator is derived as follows:

$$\sigma_{xx} - (e_0 a)^2 \frac{\partial^2 \sigma_{xx}}{\partial x^2} = \tau_{xx} \quad \text{where} \quad \tau_{xx} = E\varepsilon_{xx} \tag{12}$$

The deposited or grabbed atomic-mass contributes to the resonator's frequencies where an additional inertia term that depends on the atomic-mass appears in the beam's characteristics equation. This additional inertia works in parallel with the mass of the resonator to form its total inertia. This can be clearly shown in the performed works by Aboelkassem et al. [51] and Shaat and Abdelkefi [5, 7]. However, in addition to its inertia contribution, the atomic-mass can affect the fields, such as moments, forces, deflections, and slopes, depending on its location. Thus, in addition to the conventional boundary conditions of the mechanical resonator, some continuity conditions should be considered at the atomic-mass location.

According to the previous discussion, the displacement field of the SWCNT is divided with respect to the atomic-mass location, x_m, as follows:

$$u(x,t) = \begin{cases} u_1(x,t), & 0 \le x \le x_m \\ u_2(x,t), & x_m < x \le L \end{cases}, \quad w(x,t) = \begin{cases} w_1(x,t), & 0 \le x \le x_m \\ w_2(x,t), & x_m < x \le L \end{cases} \tag{13}$$

To derive the equations of motion of the SWCNT-mass sensor, the Hamilton's principle is used which states:

$$\delta H = \int_{t_1}^{t_2} (\delta T_b + \delta T_m - \delta \Pi) \mathrm{d}t = 0 \tag{14}$$

where T_b and T_m are, respectively, the kinetic energy of the SWCNT and the kinetic energy of the atomic-mass. Π denotes the total potential energy of the SWCNT.

For a free vibration analysis of the resonator, the forcing terms in Eq. (5) are omitted. Consequently, the first variation of the total potential energy of the resonator can be expressed as:

$$\begin{aligned} \delta \Pi &= \int_0^L \int_A \sigma_{xx} \delta \varepsilon_{xx} \mathrm{d}A \mathrm{d}x \\ &= \int_0^{x_m} \left[N_1 \delta \left(u_1' + \frac{1}{2}(w_1')^2 \right) - M_1 \delta w_1'' \right] \mathrm{d}x \\ &\quad + \int_{x_m}^{L} \left[N_2 \delta \left(u_2' + \frac{1}{2}(w_2')^2 \right) - M_2 \delta w_1'' \right] \mathrm{d}x \end{aligned} \tag{15}$$

where N_1, i.e., $0 \le x \le x_m$, and N_2, i.e., $x_m \le x \le L$, are the nonlocal axial force resultants through the beam span. $M_1(x)$, i.e., $0 \le x \le x_m$, and $M_2(x)$, i.e., $x_m \le x \le L$, are

the nonlocal bending moment resultants. These stress resultants can be expressed in terms of the nonlocal stress as follows:

$$N_{1,2} = \int_A (\sigma_{xx})_{1,2} \mathrm{d}A, \quad M_{1,2} = \int_A z(\sigma_{xx})_{1,2} \mathrm{d}A \tag{16}$$

Therefore, by integrating both sides of Eq. (12) over the cross-sectional area, A, of the beam,

$$\begin{aligned} &\int_A \sigma_{xx} \mathrm{d}A - (e_0 a)^2 \frac{\partial^2}{\partial x^2} \int_A \sigma_{xx} \mathrm{d}A = E \int_A \varepsilon_{xx} \mathrm{d}A \\ &\int_A z\sigma_{xx} \mathrm{d}A - (e_0 a)^2 \frac{\partial^2}{\partial x^2} \int_A z\sigma_{xx} \mathrm{d}A = E \int_A z\varepsilon_{xx} \mathrm{d}A \end{aligned} \tag{17}$$

and by substituting for the strain from Eq. (11) into Eq. (12), the nonlocal stress resultants can be derived in terms of the axial and the transverse displacements as follows:

$$N_{1,2} - (e_0 a)^2 N''_{1,2} = EA\left(u'_{1,2} + \frac{1}{2}\left(w'_{1,2}\right)^2\right) \tag{18a}$$

$$M_{1,2} - (e_0 a)^2 M'_{1,2} = -EIw''_{1,2} \tag{18b}$$

where I denotes the second area moment of inertia of the SWCNT and A represents the cross-sectional area.

The first variation of the kinetic energy of the SWCNT-resonator, δT_b, and the atomic-mass particle, δT_m, can be defined as follows:

$$\begin{aligned} \delta T_b &= \int_0^L \int_A \rho \dot{w} \delta \dot{w} dA dx \\ &= \int_0^{x_m} m_0 \dot{w}_1 \delta \dot{w}_1 dx + \int_{x_m}^L m_0 \dot{w}_2 \delta \dot{w}_2 dx \end{aligned} \tag{19}$$

$$\delta T_m = m(\dot{w}_1 \delta \dot{w}_1)_{x=x_m} \tag{20}$$

where ρ is the mass density of the SWCNT and $m_0 = \rho A$ denotes the mass per unit length of the resonator. m represents the mass of the deposited atomic particle. The $\dot{(\cdot)}$ denotes partial differentiation with respect to time t.

Substituting Eqs. (15), (19), and (20) into Eq. (14) and using the standard variation techniques, the following variations are obtained:

$$\begin{aligned} \int_{t_1}^{t_2} \delta \Pi \mathrm{d}t = &\int_{t_1}^{t_2} \left(N_1 \delta u_1 \big|_0^{x_m} + N_1 w'_1 \delta w_1 \big|_0^{x_m} - M_1 \delta w'_1 \big|_0^{x_m} + M'_1 \delta w_1 \big|_0^{x_m}\right) \mathrm{d}t \\ &+ \int_{t_1}^{t_2} \left(N_2 \delta u_2 \big|_{x_m}^{L} + N_2 w'_2 \delta w_2 \big|_{x_m}^{L} - M_2 \delta w'_2 \big|_{x_m}^{L} + M'_2 \delta w_2 \big|_{x_m}^{L}\right) \mathrm{d}t \\ &+ \int_{t_1}^{t_2} \left[- \int_0^{x_m} N'_1 \delta u_1 \mathrm{d}x - \int_0^{x_m} \left(N_1 w'_1\right)' \delta w_1 \mathrm{d}x \right. \\ &\left. - \int_0^{x_m} M''_1 \delta w_1 \mathrm{d}x \right] \mathrm{d}t + \int_{t_1}^{t_2} \left[- \int_{x_m}^{L} N'_2 \delta u_2 \mathrm{d}x \right. \\ &\left. - \int_{x_m}^{L} \left(N_2 w'_2\right)' \delta w_2 \mathrm{d}x - \int_{x_m}^{L} M''_2 \delta w_2 \mathrm{d}x \right] \mathrm{d}t \end{aligned} \tag{21}$$

$$\begin{aligned} \int_{t_1}^{t_2} \delta T_b \mathrm{d}t = &\int_0^{x_m} \left(m_0 \dot{w}_1 \delta w_1 \big|_{t_1}^{t_2}\right) \mathrm{d}x + \int_0^{x_m} \left(- \int_{t_1}^{t_2} m_0 \ddot{w}_1 \delta w_1 \mathrm{d}t \right) \mathrm{d}x \\ &+ \int_{x_m}^{L} \left(m_0 \dot{w}_2 \delta w_2 \big|_{t_1}^{t_2}\right) \mathrm{d}x + \int_{x_m}^{L} \left(- \int_{t_1}^{t_2} m_0 \ddot{w}_2 \delta w_2 \mathrm{d}t \right) \mathrm{d}x \end{aligned} \tag{22}$$

$$\int_{t_1}^{t_2} \delta T_m \mathrm{d}t = m\dot{w}_1 \delta w_1 \big|_{t_1}^{t_2} - \int_{t_1}^{t_2} m\ddot{w}_1 \delta w_1 \mathrm{d}t \tag{23}$$

then, the governing equations of motion are derived as:

$$N'_1 = N'_2 = 0 \tag{24a}$$

$$-m_0 \ddot{w}_1 + M''_1 + \left(N_1 w'_1\right)' = 0 \tag{24b}$$

$$-m_0 \ddot{w}_2 + M''_2 + \left(N_2 w'_2\right)' = 0 \tag{24c}$$

and the associated boundary conditions and continuity equations for the clamped–clamped SWCNT can be defined as follows:

$$\begin{aligned} &u_1 = 0, \quad w_1 = w'_1 = 0 \quad \text{at} \quad x = 0, \quad u_2 = 0, \\ &w_2 = w'_2 = 0 \quad \text{at} \quad x = L \end{aligned} \tag{25}$$

$$\begin{aligned} &u_1 = u_2, \quad w_1 = w_2, \quad w'_1 = w'_2, \quad M_1 = M_2, \\ &N_1 = N_2 \quad \text{at} \quad x = x_m \\ &M'_2 + N_2 w'_2 - M'_1 - N_1 w'_1 - m\ddot{w}_1 = 0 \Rightarrow M'_2 - M'_1 - m\ddot{w}_1 \\ &= 0 \quad \text{at} \quad x = x_m \end{aligned} \tag{26}$$

Equation (25) presents the boundary conditions at the beam ends. Equation (26) introduces the continuity conditions at the atomic-mass location where the inertia of the atomic-mass affects the beam shear force resultant.

To form the axial force resultant, N, Eq. (24a) is substituted into Eq. (18a) to give:

$$N_{1,2} = EA\left(u'_{1,2} + \frac{1}{2}\left(w'_{1,2}\right)^2\right) \tag{27}$$

According to Eq. (24a), the axial force resultant N should be constant. Therefore, it can be formed as the induced axial force due to the beam axial stretching [52, 53]. By integrating Eq. (27) over the beam's length, one obtains:

$$\begin{aligned} &EAu_1(x_m) - EAu_1(0) + EAu_2(L) - EAu_2(x_m) \\ &+ \frac{EA}{2} \int_0^{x_m} \left[w'_1(\xi)\right]^2 \mathrm{d}\xi + \frac{EA}{2} \int_{x_m}^{L} \left[w'_2(\xi)\right]^2 \mathrm{d}\xi \\ &= N_1 x_m + N_2 L - N_2 x_m \end{aligned} \tag{28}$$

where ξ is a dummy variable.

Considering the defined boundary conditions and continuity equations (Eqs. (25, 26)) of the considered beam, the axial stress resultant $N_{1,2}$ can be extracted from Eq. (28) and can be expressed as follows:

$$N_{1,2} = \frac{EA}{2L} \int_0^{x_m} \left(w'_1\right)^2 \mathrm{d}x + \frac{EA}{2L} \int_{x_m}^{L} \left(w'_2\right)^2 \mathrm{d}x \tag{29}$$

Similarly, substituting Eqs. (24b) and (24c) into Eq. (18b) gives the bending moment resultant in the form:

$$M_{1,2} = (e_0 a)^2 \left(m_0 \ddot{w}_{1,2} - \left(N_{1,2} w'_{1,2} \right)' \right) - EI w''_{1,2} \tag{30}$$

Then, by substituting Eqs. (29) and (30) into Eqs. (24b) and (24c), the equations of motion of the SWCNT-resonator can be derived in terms of the beam's transverse displacement (deflection) as follows:

$$EI w_1'''' + m_0 \ddot{w}_1 - \left(\frac{EA}{2L} \int_0^{x_m} (w'_1)^2 \mathrm{d}x + \frac{EA}{2L} \int_{x_m}^{L} (w'_2)^2 \mathrm{d}x \right) w''_1 - (e_0 a)^2 \left[m_0 \ddot{w}''_1 - \left(\frac{EA}{2L} \int_0^{x_m} (w'_1)^2 \mathrm{d}x + \frac{EA}{2L} \int_{x_m}^{L} (w'_2)^2 \mathrm{d}x \right) w''''_1 \right] = 0 \tag{30a}$$

$$EI w_2'''' + m_0 \ddot{w}_2 - \left(\frac{EA}{2L} \int_0^{x_m} (w'_1)^2 \mathrm{d}x + \frac{EA}{2L} \int_{x_m}^{L} (w'_2)^2 \mathrm{d}x \right) w''_2 - (e_0 a)^2 \left[m_0 \ddot{w}''_2 - \left(\frac{EA}{2L} \int_0^{x_m} (w'_1)^2 \mathrm{d}x + \frac{EA}{2L} \int_{x_m}^{L} (w'_2)^2 \mathrm{d}x \right) w''''_2 \right] = 0 \tag{30b}$$

Moreover, the boundary conditions and the continuity conditions can be expressed in terms of deflection as:

$$w_1 = w'_1 = 0 \quad \text{at} \quad x = 0, \quad w_2 = w'_2 = 0 \quad \text{at} \quad x = L \tag{31a}$$

$$\begin{aligned} &w_1 = w_2, \quad w'_1 = w'_2, \quad w''_1 = w''_2 \quad \text{at} \quad x = x_m \\ &EI w'''_1 - EI w'''_2 + (e_0 a)^2 \\ &\left[\left(\frac{EA}{2L} \int_0^{x_m} (w'_1)^2 \mathrm{d}x + \frac{EA}{2L} \int_{x_m}^{L} (w'_2)^2 \mathrm{d}x \right) (w'''_1 - w'''_2) \right] \\ &- m \ddot{w}_1 = 0 \quad \text{at} \quad x = x_m \end{aligned} \tag{31b}$$

It should be noted that $\ddot{w}_1 = \ddot{w}_2, \quad \text{at} \quad x = x_m$, that is why the continuity conditions in Eq. (31b) are obtained in this form. In the current study, the following dimensionless quantities are introduced to normalize the derived equations of motion and boundary conditions:

$$\begin{aligned} &\chi = x/L, \quad W_{1,2} = w_{1,2}\sqrt{A/I}, \quad \tau = \sqrt{EI/m_0 L^4}\, t, \\ &\omega = \omega^* \Big/ \sqrt{EI/m_0 L^4}, \quad e = e_0 a/L, \quad \eta = x_m/L, \alpha = m/m_0 L \end{aligned} \tag{32}$$

where ω^* is the dimensional natural frequency of SWCNT-resonator. Equations (30) and (31) can be rewritten in the dimensionless form as:

$$\frac{\partial^4 W_1}{\partial \chi^4} + \frac{\partial^2 W_1}{\partial \tau^2} - \left(\frac{1}{2} \int_0^{\eta} \left(\frac{\partial W_1}{\partial \chi} \right)^2 \mathrm{d}\chi + \frac{1}{2} \int_{\eta}^{1} \left(\frac{\partial W_2}{\partial \chi} \right)^2 \mathrm{d}\chi \right) \frac{\partial^2 W_1}{\partial \chi^2} - e^2 \left[\frac{\partial^4 W_1}{\partial \chi^2 \partial \tau^2} - \left(\frac{1}{2} \int_0^{\eta} \left(\frac{\partial W_1}{\partial \chi} \right)^2 \mathrm{d}\chi + \frac{1}{2} \int_{\eta}^{1} \left(\frac{\partial W_2}{\partial \chi} \right)^2 \mathrm{d}\chi \right) \frac{\partial^4 W_1}{\partial \chi^4} \right] = 0 \tag{33a}$$

$$\frac{\partial^4 W_2}{\partial \chi^4} + \frac{\partial^2 W_2}{\partial \tau^2} - \left(\frac{1}{2} \int_0^{\eta} \left(\frac{\partial W_1}{\partial \chi} \right)^2 \mathrm{d}\chi + \frac{1}{2} \int_{\eta}^{1} \left(\frac{\partial W_2}{\partial \chi} \right)^2 \mathrm{d}\chi \right) \frac{\partial^2 W_2}{\partial \chi^2} - e^2 \left[\frac{\partial^4 W_2}{\partial \chi^2 \partial \tau^2} - \left(\frac{1}{2} \int_0^{\eta} \left(\frac{\partial W_1}{\partial \chi} \right)^2 \mathrm{d}\chi + \frac{1}{2} \int_{\eta}^{1} \left(\frac{\partial W_2}{\partial \chi} \right)^2 \mathrm{d}\chi \right) \frac{\partial^4 W_2}{\partial \chi^4} \right] = 0 \tag{33b}$$

$$W_1 = W'_1 = 0 \quad \text{at} \quad \chi = 0, \quad W_2 = W'_2 = 0 \quad \text{at} \quad \chi = 1 \tag{34a}$$

$$\begin{aligned} &W_1 = W_2, \quad W'_1 = W'_2, \quad W''_1 = W''_2 \quad \text{at} \quad \chi = \eta \\ &\frac{\partial^3 W_1}{\partial \chi^3} - \frac{\partial^3 W_2}{\partial \chi^3} + e^2 \\ &\left[\left(\frac{1}{2} \int_0^{\eta} \left(\frac{\partial W_1}{\partial \chi} \right)^2 \mathrm{d}\chi + \frac{1}{2} \int_{\eta}^{1} \left(\frac{\partial W_2}{\partial \chi} \right)^2 \mathrm{d}\chi \right) \left(\frac{\partial^3 W_1}{\partial \chi^3} - \frac{\partial^3 W_2}{\partial \chi^3} \right) \right] \\ &- \alpha \frac{\partial^2 W_1}{\partial \tau^2} = 0 \quad \text{at} \quad \chi = \eta \end{aligned} \tag{34b}$$

Usually, when the CNT size is much higher than the atomic lattice parameter of its unit cells ($L \gg a$), the contribution of the nonlocal residual to the CNT behavior is negligible. By inspecting Eqs. (33) and (34), it is clear that when $L \gg a$, the derived equations of motions and boundary conditions reduce to the classical ones where $e \ll 1$.

3.2 Determination of the natural frequencies and mode shapes

To determine the natural frequencies and mode shapes of the SWCNT-resonator, the beam's deflection is decomposed as:

$$W_1 = \Phi_1(\chi) e^{i\omega\tau}, \quad W_2 = \Phi_2(\chi) e^{i\omega\tau} \tag{35}$$

where $\Phi_1(\chi)$ and $\Phi_2(\chi)$ are the nondimensional mode shape functions of the resonator. ω denotes the nondimensional natural frequency.

The substitution of Eq. (35) into Eqs. (33) and (34) gives:

$$\frac{\partial^4 \Phi_1}{\partial \chi^4} - \omega^2 \Phi_1 - \left(\frac{1}{2} \int_0^{\eta} \left(\frac{\partial \Phi_1}{\partial \chi} \right)^2 \mathrm{d}\chi + \frac{1}{2} \int_{\eta}^{1} \left(\frac{\partial \Phi_2}{\partial \chi} \right)^2 \mathrm{d}\chi \right) \frac{\partial^2 \Phi_1}{\partial \chi^2} e^{2i\omega\tau} + e^2 \left[\omega^2 \frac{\partial^2 \Phi_1}{\partial \chi^2} + \left(\frac{1}{2} \int_0^{\eta} \left(\frac{\partial \Phi_1}{\partial \chi} \right)^2 \mathrm{d}\chi + \frac{1}{2} \int_{\eta}^{1} \left(\frac{\partial \Phi_2}{\partial \chi} \right)^2 \mathrm{d}\chi \right) \frac{\partial^4 \Phi_1}{\partial \chi^4} e^{2i\omega\tau} \right] = 0 \tag{36a}$$

$$\frac{\partial^4 \Phi_2}{\partial \chi^4} - \omega^2 \Phi_2 - \left(\frac{1}{2} \int_0^{\eta} \left(\frac{\partial \Phi_1}{\partial \chi} \right)^2 \mathrm{d}\chi + \frac{1}{2} \int_{\eta}^{1} \left(\frac{\partial \Phi_2}{\partial \chi} \right)^2 \mathrm{d}\chi \right) \frac{\partial^2 \Phi_2}{\partial \chi^2} e^{2i\omega\tau} + e^2 \left[\omega^2 \frac{\partial^2 \Phi_2}{\partial \chi^2} + \left(\frac{1}{2} \int_0^{\eta} \left(\frac{\partial \Phi_1}{\partial \chi} \right)^2 \mathrm{d}\chi + \frac{1}{2} \int_{\eta}^{1} \left(\frac{\partial \Phi_2}{\partial \chi} \right)^2 \mathrm{d}\chi \right) \frac{\partial^4 \Phi_2}{\partial \chi^4} e^{2i\omega\tau} \right] = 0 \tag{36b}$$

$$\Phi_1 = \Phi_1' = 0 \quad \text{at} \quad \chi = 0, \quad \Phi_2 = \Phi_2' = 0 \quad \text{at} \quad \chi = 1 \tag{37a}$$

$$\Phi_1 = \Phi_2, \quad \Phi_1' = \Phi_2', \quad \Phi_1'' = \Phi_2'' \quad \text{at} \quad \chi = \eta$$
$$\frac{\partial^3 \Phi_1}{\partial \chi^3} - \frac{\partial^3 \Phi_2}{\partial \chi^3} + e^2 \left[\left(\frac{1}{2} \int_0^\eta \left(\frac{\partial \Phi_1}{\partial \chi} \right)^2 \mathrm{d}\chi + \frac{1}{2} \int_\eta^1 \left(\frac{\partial \Phi_2}{\partial \chi} \right)^2 \mathrm{d}\chi \right) \left(\frac{\partial^3 \Phi_1}{\partial \chi^3} - \frac{\partial^3 \Phi_2}{\partial \chi^3} \right) e^{2i\omega\tau} \right] + \alpha\omega^2 \Phi_1 = 0 \quad \text{at} \quad \chi = \eta \tag{37b}$$

In order to proceed with the eigenvalue problem analysis, the nonlinear terms in Eqs. (36) and (37) should be omitted. Therefore, the linearized version of the equation of motion and boundary conditions can be expressed as follows:

$$\frac{\partial^4 \Phi_1}{\partial \chi^4} - \omega^2 \Phi_1 + e^2 \omega^2 \frac{\partial^2 \Phi_1}{\partial \chi^2} = 0 \tag{38a}$$

$$\frac{\partial^4 \Phi_2}{\partial \chi^4} - \omega^2 \Phi_2 + e^2 \omega^2 \frac{\partial^2 \Phi_2}{\partial \chi^2} = 0 \tag{38b}$$

$$\Phi_1(0) = \frac{\partial \Phi_1(0)}{\partial \chi} = 0, \quad \Phi_2(1) = \frac{\partial \Phi_2(1)}{\partial \chi} = 0 \tag{39a}$$

$$\Phi_1(\eta) = \Phi_2(\eta), \quad \frac{\partial \Phi_1(\eta)}{\partial \chi} = \frac{\partial \Phi_2(\eta)}{\partial \chi}, \quad \frac{\partial^2 \Phi_1(\eta)}{\partial \chi^2} = \frac{\partial^2 \Phi_2(\eta)}{\partial \chi^2}$$
$$\frac{\partial^3 \Phi_1(\eta)}{\partial \chi^3} - \frac{\partial^3 \Phi_2(\eta)}{\partial \chi^3} + \alpha\omega^2 \Phi_1(\eta) = 0 \tag{39b}$$

The general solutions for Eqs. (38a) and (38b) can be expressed in the form:

$$\Phi_1(\chi) = C_1 \sin(\lambda\kappa_1\chi) + C_2 \cos(\lambda\kappa_1\chi) + C_3 \sinh(\lambda\kappa_2\chi) + C_4 \cosh(\lambda\kappa_2\chi) \tag{40a}$$

$$\Phi_2(\chi) = C_5 \sin(\lambda\kappa_1\chi) + C_6 \cos(\lambda\kappa_1\chi) + C_7 \sinh(\lambda\kappa_2\chi) + C_8 \cosh(\lambda\kappa_2\chi) \tag{40b}$$

where

$$\begin{Bmatrix} \kappa_1 \\ \kappa_2 \end{Bmatrix} = \sqrt{\frac{\sqrt{e^4\lambda^4 + 4} \pm e^2\lambda^2}{2}}, \quad \lambda = \sqrt{\omega} \tag{41}$$

The constants $C_1 - C_8$ can be obtained by applying the boundary conditions (Eq. (39a)) and the continuity conditions (39b). By considering the following relations:

$$\kappa_1\kappa_2 = 1, \quad \kappa_1^2 + \kappa_2^2 = \sqrt{e^4\lambda^4 + 4}, \quad \kappa_1^2 - \kappa_2^2 = e^2\lambda^2 \tag{42}$$

The exact mode shapes of the SWCNT-resonator can be then derived as:

$$\Phi_1 = C\{A_1(\cos\lambda\kappa_1\chi - \cosh\lambda\kappa_2\chi) - A_2(\sin\lambda\kappa_1\chi - \kappa_1^2 \sinh\lambda\kappa_2\chi)\} \tag{43a}$$

$$\Phi_2 = C \begin{Bmatrix} B_1 \sin\lambda\kappa_1\chi + B_1(-\cosh\lambda\kappa_2 \sin\lambda\kappa_1 + \kappa_1^2 \cos\lambda\kappa_1 \sinh\lambda\kappa_2)\cosh\lambda\kappa_2\chi \\ + B_1(-\kappa_1^2 \cos\lambda\kappa_1 \cosh\lambda\kappa_2 + \sin\lambda\kappa_1 \sinh\lambda\kappa_2)\sinh\lambda\kappa_2\chi + B_2 \cos\lambda\kappa_1\chi \\ - B_2(\cos\lambda\kappa_1 \cosh\lambda\kappa_2(1-\chi) + \kappa_1^2 \sin\lambda\kappa_1 \sinh\lambda\kappa_2(1-\chi)) \end{Bmatrix} \tag{43b}$$

where

$$\begin{aligned}
A_1 =& \cosh\lambda\kappa_2(1-\eta)\sin\lambda\kappa_1 - \sin\lambda\kappa_1\eta \\
&- \cosh\lambda\kappa_2 \sin\lambda\kappa_1(1-\eta) \\
&+ \kappa_1^2 \cos\lambda\kappa_1(1-\eta)\sinh\lambda\kappa_2 - \kappa_1^2 \sinh\lambda\kappa_2\eta \\
&- \kappa_1^2 \cos\lambda\kappa_1 \sinh\lambda\kappa_2(1-\eta) \\
A_2 =& -\cos\lambda\kappa_1\eta + \cos\lambda\kappa_1(1-\eta)\cosh\lambda\kappa_2 - \cosh\lambda\kappa_2\eta \\
&+ \cos\lambda\kappa_1 \cosh\lambda\kappa_2(1-\eta) - \kappa_2^2 \sin\lambda\kappa_1(1-\eta) \\
&\sinh\lambda\kappa_2 + \kappa_1^2 \sin\lambda\kappa_1 \sinh\lambda\kappa_2(1-\eta) \\
B_1 =& -\cos\lambda\kappa_1\eta + \cos\lambda\kappa_1(1+\eta)\cosh\lambda\kappa_2 + \cosh\lambda\kappa_2\eta \\
&- \cos\lambda\kappa_1 \cosh\lambda\kappa_2(1-\eta) \\
&+ (\kappa_1^2 \cos\lambda\kappa_1\eta \sin\lambda\kappa_1 - \kappa_2^2 \sin\lambda\kappa_1\eta \cos\lambda\kappa_1)\sinh\lambda\kappa_2 \\
&- \kappa_1^2 \sin\lambda\kappa_1 \sinh\lambda\kappa_2(1-\eta) \\
B_2 =& \cosh\lambda\kappa_2(1-\eta)\sin\lambda\kappa_1 + \sin\lambda\kappa_1\eta \\
&- \cosh\lambda\kappa_2 \sin\lambda\kappa_1(1+\eta) \\
&+ (\kappa_1^2 \cos\lambda\kappa_1\eta \cos\lambda\kappa_1 + \kappa_2^2 \sin\lambda\kappa_1\eta \sin\lambda\kappa_1) \\
&\sinh\lambda\kappa_2 - \kappa_1^2 \sinh\lambda\kappa_2\eta - \kappa_1^2 \cos\lambda\kappa_1 \sinh\lambda\kappa_2(1-\eta)
\end{aligned}$$

The constant C in Eq. (43) can be obtained using the normalization condition:

$$\int_0^\eta \Phi_1^2 \mathrm{d}\chi + \int_\eta^1 \Phi_2^2 \mathrm{d}\chi = 1 \tag{44}$$

The natural frequencies can be determined from the following characteristic equation:

$$\begin{aligned}
&-2\kappa_1\sqrt{e^4\lambda^4 + 4} + 2\kappa_1\sqrt{e^4\lambda^4 + 4}\cos\lambda\kappa_1 \cosh\lambda\kappa_2 \\
&+ \kappa_1 e^2\lambda^2\sqrt{e^4\lambda^4 + 4}\sin\lambda\kappa_1 \sinh\lambda\kappa_2 \\
&+ \alpha\lambda\{2\cosh\lambda\kappa_2\eta \sin\lambda\kappa_1\eta - \cosh\lambda\kappa_2 \sin\lambda\kappa_1 \\
&+ 2\sin\lambda\kappa_1(1-\eta)\cosh\lambda\kappa_2(1-\eta) \\
&- 2\kappa_1^2 \sinh\lambda\kappa_2(1-\eta)\cos\lambda\kappa_1(1-\eta) \\
&+ (\kappa_1^2 \cos\lambda\kappa_1(1-\eta)\cos\lambda\kappa_1\eta + \kappa_2^2 \sin\lambda\kappa_1(1-\eta) \\
&\times \sin\lambda\kappa_1\eta)\sinh\lambda\kappa_2 - 2\kappa_1^2 \cos\lambda\kappa_1\eta \sinh\lambda\kappa_2\eta \\
&+ \kappa_1^2 \cos\lambda\kappa_1 \sinh\lambda\kappa_2 - (\cosh\lambda\kappa_2(1-\eta) \\
&\times \cosh\lambda\kappa_2\eta - \kappa_1^4 \sinh\lambda\kappa_2(1-\eta)\sinh\lambda\kappa_2\eta)\sin\lambda\kappa_1\} = 0
\end{aligned} \tag{45}$$

4 Results and discussions

The ability of CNTs as mechanical resonators used to detect the mass of atoms is investigated. To this aim, a clamped–clamped SWCNT is considered and the proposed accurate model is utilized to perform the next analyses. First, a parametric study is carried out to investigate the effects of the location of the deposited mass, the resonator's size, and the nonlocal residuals on the natural frequencies and mode shapes of the CNT-resonator. Second, the sensitivity of the proposed SWCNT-resonator for atomic-mass sensing is assessed for different noble gas particles.

4.1 Impacts of the location of the deposited mass and nonlocal parameter on the natural frequencies and mode shapes

Chiu et al. [17] developed a clamped–clamped CNT-based nano-mechanical resonator as an atomic-mass sensor to measure the mass of Xe gas atoms assuming the atom to be deposited at the middle point of the CNT-resonator. In addition, Li et al. [37] studied the dynamic behavior of clamped–clamped CNT-based mass sensors via a nonlocal Euler–Bernoulli beam model assuming the atomic-mass to be landed at the middle span of the CNT. As we previously mentioned, atomic-masses can be deposited at any location through the span of the CNT. Thus, the proposed models for CNTs-based mass sensors should account for the effects of the inertia and the arbitrary location of the deposited atomic-mass on the resonator's natural frequencies and its accuracy for mass detection.

Next, a zigzag (10, 0) SWCNT-based mechanical resonator is considered with diameter $D \approx 0.8$ nm, axial length $L = 10$ nm, density $\rho = 2.3$ g/gcm^3 cm^3, Young's modulus $E = 1$ TPa, and wall thickness $h = 0.34$ nm [30]. The cross-sectional area A and the area moment of inertia I of the resonator can be defined in terms of the diameter and the wall thickness of the CNT as:

$$\begin{aligned} A &= \pi/4\left[(D+h)^2-(D-h)^2\right] \\ I &= \pi/64\left[(D+h)^4-(D-h)^4\right] \end{aligned} \tag{46}$$

A single Xe-atom with a mass and a diameter of 0.218 zg and 322 pm, respectively, is deposited on the resonator's surface. In the developed model, the nonlocal elasticity is employed to capture the effects of the interatomic interactions on the resonators sensitivity and accuracy for mass detection. The value of the nonlocal parameter e_0a for carbon nanotubes has been represented as $e_0a \leq 2$ nm [32]. The internal characteristic length (the atomic lattice length) is represented as $a = 0.142$ nm which denotes the length of a carbon–carbon covalent bond in the atomistic lattice of SWCNTs. It should be noted that if the nonlocal parameter is set equal to zero, i.e., $e_0a = 0$, the nonlocal Euler–Bernoulli beam model converts to its classical counterpart.

The plotted curves in Fig. 2 show the induced shifts in the SWCNT natural frequencies due to the addition of a single Xe-atom. Moreover, these plots address the influences of the location of the deposited atomic-mass on the frequency shifts of the CNT-resonator. The horizontal lines in Fig. 2a–c refer to the CNT natural frequencies when no masses are added to the mechanical resonator. Inspecting the plotted curves in Fig. 2a, a high shift of 16.5 GHz is obtained in the first natural frequency of the resonator when the atomic-scale Xe-mass is deposited in the mid-span ($\eta = 0.5$) of the clamped–clamped CNT-resonator. In addition, a 26.5-GHz second mode frequency shift can be obtained when the atomic-mass is deposited at $\eta = 0.3$ or $\eta = 0.7$, as shown in Fig. 2b. It follows from Fig. 2c that two different frequency shifts in the third natural frequency of the resonator, respectively, 22.5 and 36.5 GHz, are obtained when the Xe atomic particle is deposited at $\eta = 0.5$ and $\eta = 0.2$ or $\eta = 0.8$, respectively.

Inspecting the obtained results in Fig. 2a–c, it can be concluded that designing mechanical resonators that operate at higher frequencies increases their sensitivities for mass sensing. Furthermore, the sensitivity of the resonator strongly depends on the location of the deposited mass. Hence, these resonators can be operated such that, depending on the location of the deposited mass, the best mode of the CNT-resonator can be selected to estimate the mass of the deposited particle. In addition, designing CNTs-resonators that operate at different vibrational modes is beneficial where the deposited mass can be located anywhere through the beam length. Thus, the vibrational mode of the device can be adjusted according to the mass location to give higher sensitivity. Moreover, the obtained results demonstrate that without knowing the exact location of the deposited particle, its estimated mass cannot be accurately determined.

To investigate the influences of the nonlocal parameter on the natural frequencies of the SWCNT-resonator, we plot in Fig. 3a–c the variations of the first three natural frequencies as functions of the location of the deposited single Xe-mass when considering three different values of the nonlocal parameter. It follows from these plots that the nonlocal parameter strongly affects the dynamic behavior of the CNT. Indeed, a significant decrease is observed in the natural frequencies of the CNT when the nonlocal parameter is increased, and hence, a reduction in the sensitivity of the CNT-based mass sensor is obtained. It is clear that modeling the CNT-resonator based on the classical model ($e_0 = 0$) results in an overestimation of the

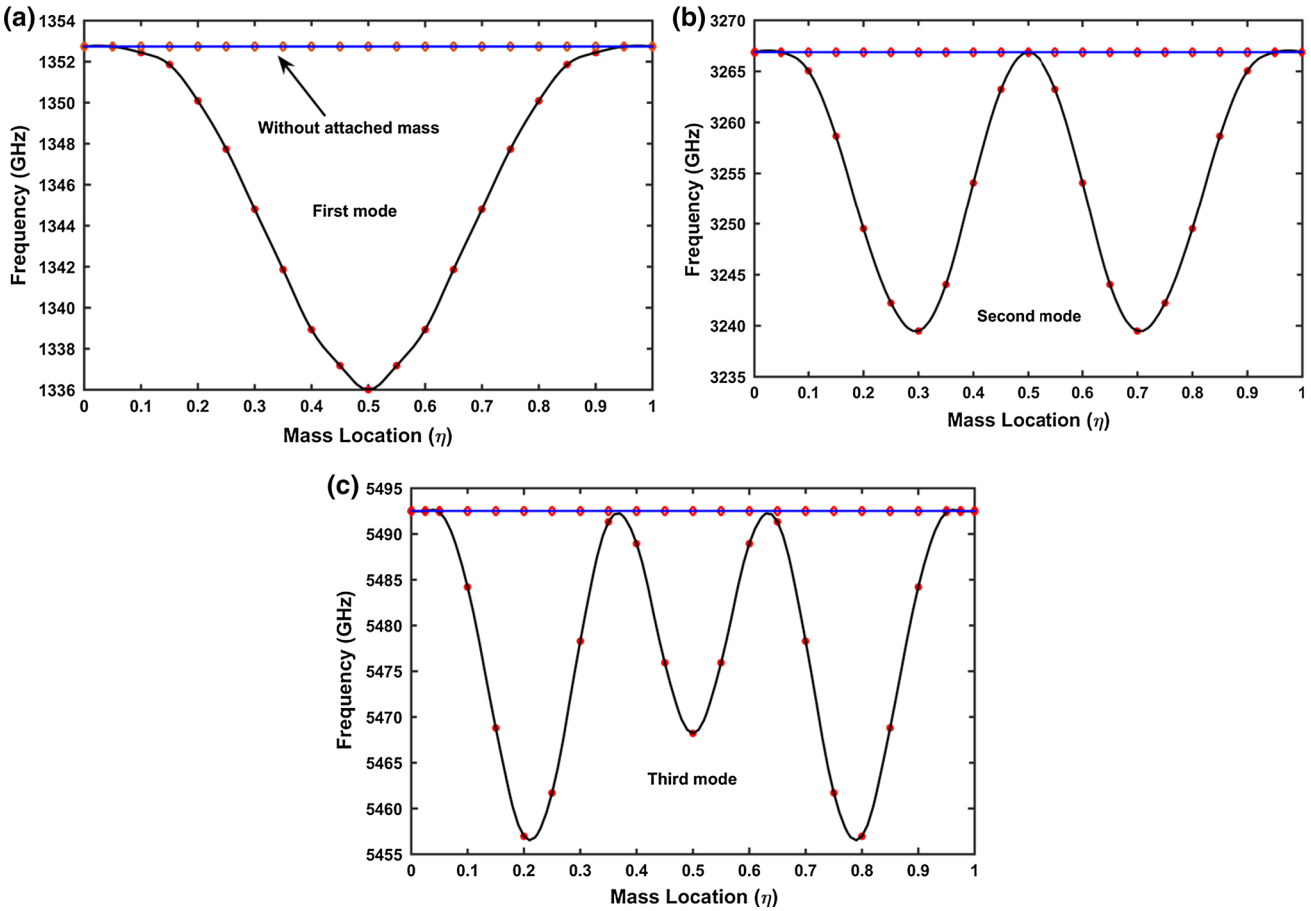

Fig. 2 Variations of the **a** first, **b** second, and **c** third natural frequencies of the SWCNT-resonator as functions of the location of the deposited Xe atomic-mass when the nonlocal parameter is set equal to $e_0 = 0.1$

deposited mass value because the classical model reflects higher frequencies when compared to the nonlocal model. Inspecting the plots in Fig. 3a–c, it is clear that the most sensitive locations of the deposited mass are independent of the nonlocal parameter.

As for the impacts of the nonlocal parameter on the first three mode shapes of the SWCNT-resonator, we plot in Figs. 4, 5, and 6 the variations of these mode shapes when considering various locations of the deposited atomic-scale mass for different nonlocal parameters. When the added mass is located in the middle of the CNT ($\eta = 0.5$), it is obvious that the nonlocal parameter has a negligible effect on the first mode shape, as shown in Fig. 4a. Zooming near the location of the deposited Xe-mass as presented in Fig. 4b, it is noted that the amplitude of the first mode shape is increased when the nonlocal parameter is increased. However, a remarkable impact is observed in the second and third mode shapes when the nonlocal parameter is varied between 0 and 0.2, as presented in Fig. 4c, d, respectively. In fact, an increase in the nonlocal parameter is accompanied by a reduction in the width between the two peaks of the second structural mode shape. In addition, a slight increase in the amplitude of the second mode shape is obtained when the nonlocal parameter is set equal to 0.2, as shown in Fig. 4c. Concerning the third mode shape, it follows from Fig. 4d that a decrease in the value of the nonlocal parameter is associated with an increase in the amplitude of this mode shape without any change in the placement of its peak.

When the atomic-scale mass is deposited at $\eta = 0.3$, the influence of the nonlocal parameter on the first and second mode shapes is negligible, as shown in Fig. 5a, c, respectively. As for the first mode shape, it follows from Fig. 5b that the amplitude does not change when increasing the nonlocal parameter from zero to 0.1. However, increasing the nonlocal parameter from 0.1 to 0.2, there is an increase in the amplitude of this mode. Concerning the second mode shape, zooming near its peak ($\eta = 0.7$), it is shown in Fig. 5d that the variation of this mode with the nonlocal parameter is so dependent on the position. Similar to the

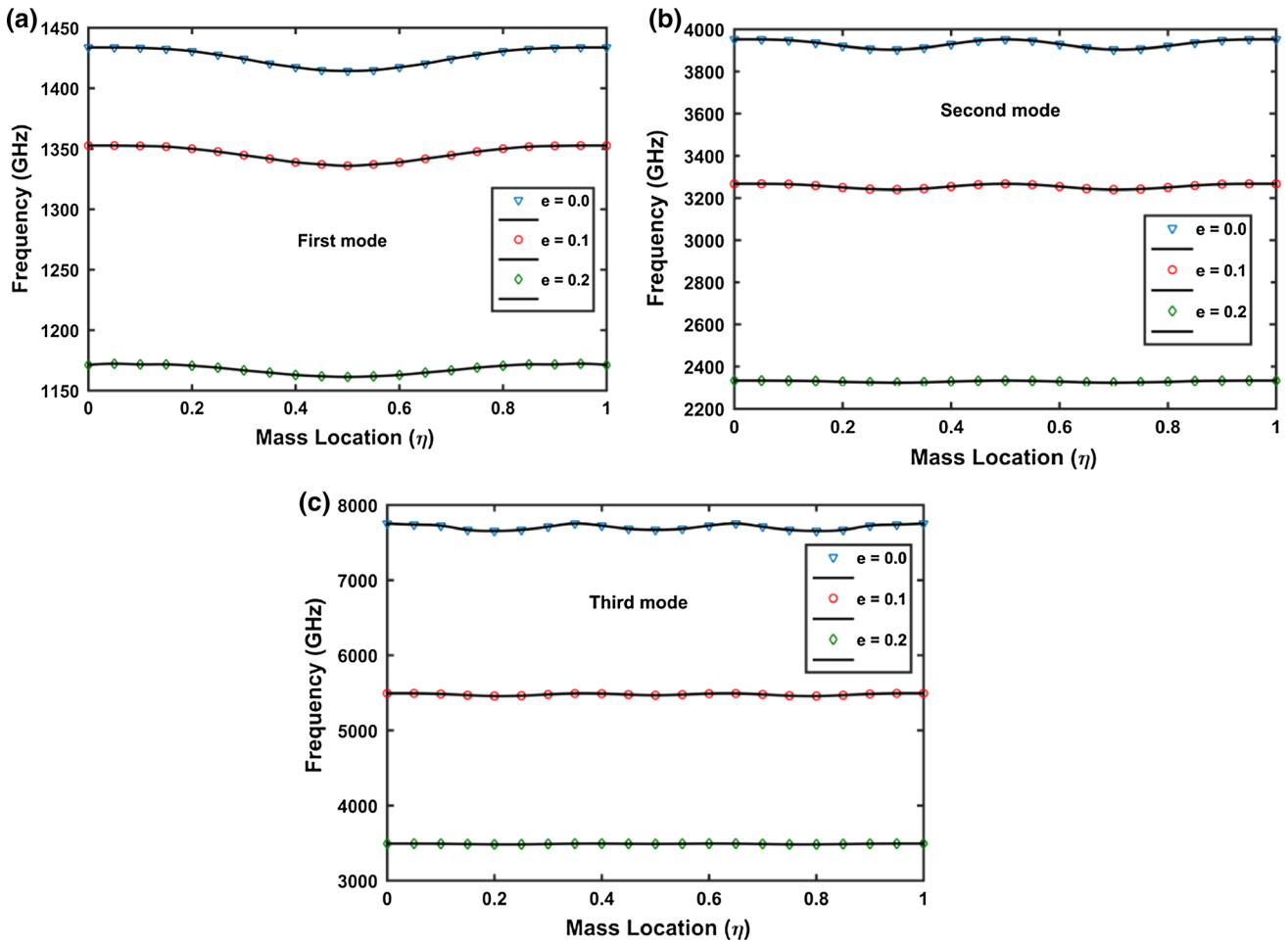

Fig. 3 Variations of the **a** first, **b** second, and **c** third natural frequencies of the SWCNT-resonator when varying the nonlocal residual parameter

case when the atomic-scale mass is deposited at $\eta = 0.5$, the third mode shape is impacted by the value of the nonlocal parameter, as shown in Fig. 5e.

Inspecting the variations of the first three mode shapes presented in Fig. 6 where the atomic-mass is deposited at $\eta = 0.1$, similar results as the case of $\eta = 0.3$ are obtained. Indeed, the nonlocal parameter acts as an amplifier for the first mode shape amplitude, as presented in Fig. 6b. As for the second mode shape of vibration, the nonlocal parameter has a negligible impact on its amplitude, as presented in Fig. 6c. When zooming near its peak, as shown in Fig. 6d, it is noted that an increase in the nonlocal parameter is accompanied by an increase in the amplitude of this mode shape. As for the behavior of the third mode shape with respect to the nonlocal parameter, it remains the same for all cases of mass locations. It is concluded that the nonlocal parameter has diverse influences on the vibration mode shapes depending on the location of the single Xe-atom. These results show the necessity of this analysis and the developed mathematical model for accurate estimation of the natural frequencies as well as the associated mode shapes of CNT-mass sensors. It should be mentioned that the developed model as well as the derived mode shapes are so needed when forced or nonlinear analyses are performed.

4.2 Sensitivity of SWCNT for different noble gases

Another important parameter which is considered in analyzing the performance of CNT-based mass sensors is called "frequency shift percent" (FSP). As it has been mentioned in [54], the FSP indicates the difference between the resonant frequency of SWCNT before and after depositing a mass as a percentage of the SWCNT's natural frequency without the attached mass which can be expressed as:

$$\mathrm{FSP} = 100 \times \frac{\omega_{\text{Without attached mass}} - \omega_{\text{With attached mass}}}{\omega_{\text{Without attached mass}}} \tag{47}$$

In Fig. 7, the variations of the FSP with respect to the nonlocal parameter and the location of the deposited single Xe-atom for the first three vibration modes of the SWCNT-resonator are plotted. Clearly, the nonlocal parameter has a

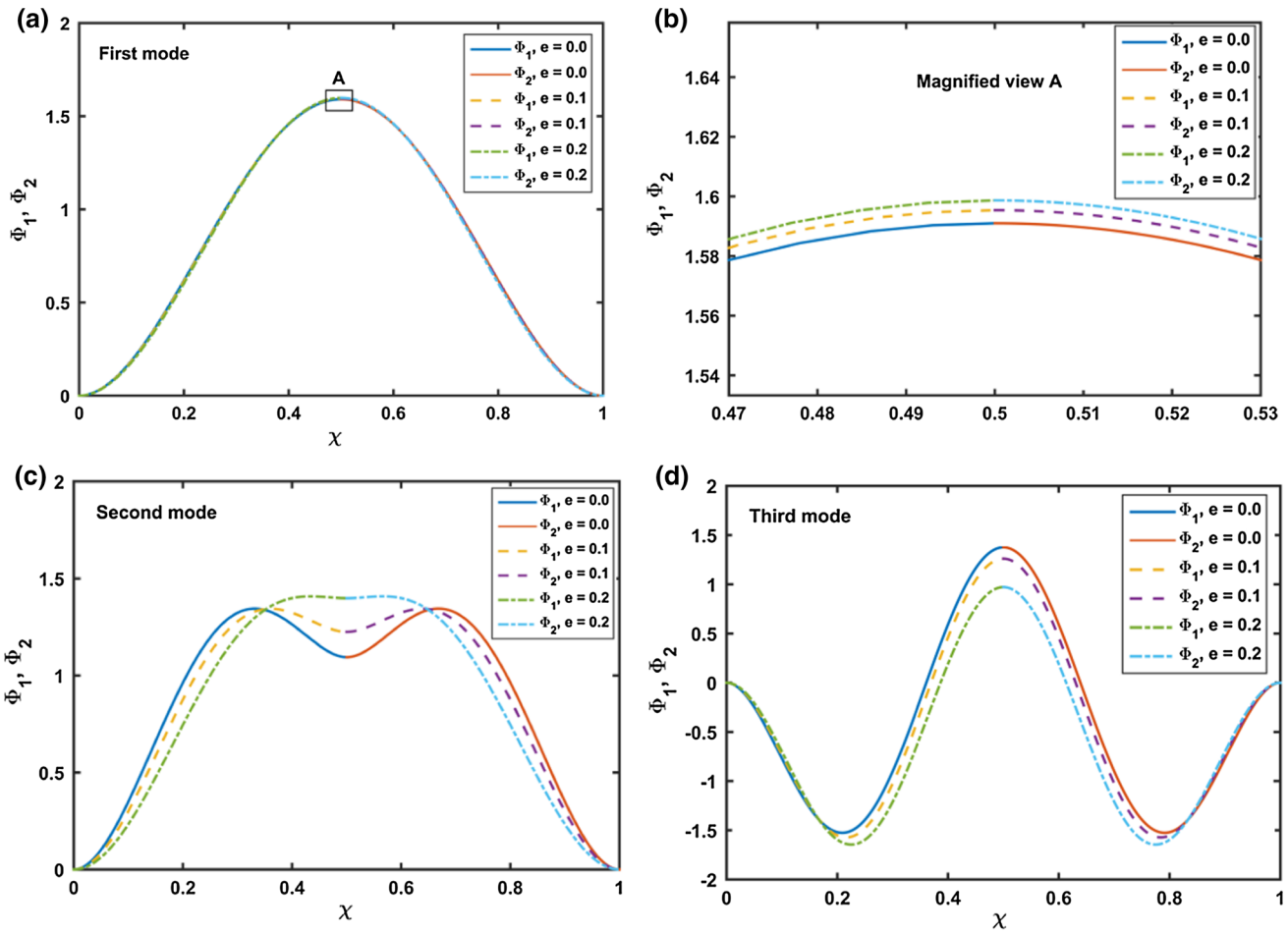

Fig. 4 Variations of the first three mode shapes of SWCNT when considering various values of the nonlocal parameter and when a single Xe-atom is deposited at $\eta = 0.5$

great impact on the FSP of the SWCNT where reductions in FSP of the second and the third vibrational modes are obtained when increasing the nonlocal parameter. For the first vibrational mode, a decrease in the FSP with the increase in the nonlocal parameter is observed when the atomic-mass is deposited at $\eta = 0.5$ and 0.3, as shown in Fig. 7a, b. On the other hand, with the increase in the nonlocal parameter, an increase in FSP of the first mode is observed when depositing the mass at $\eta = 0.1$. These obtained trends assure the importance of considering the coupled effects of the nonlocal and the atomic-mass position.

In Fig. 8a, b, we plot the FSP when noble gas atoms Ar and He are deposited on the top of the SWCNT-resonator at $\eta = 0.5$. As previously demonstrated, the second vibrational mode is not useful to estimate a deposited mass when $\eta = 0.5$ where it gives a zero frequency shift. To investigate the effects of the nonlocal parameter on the frequencies of the CNT-resonator, the FSP for different nonlocal parameters is compared to the ones obtained according to the classical model ($e_0 = 0$). Clearly, almost 92 and 100 % reductions in the third mode frequency are obtained when increasing the nonlocal parameter from 0 to 0.2 for the Ar and the He atoms, respectively. Compared with the SWCNT-Xe, the FSP of both SWCNT-Ar and SWCNT-He is much lower than the SWCNT-Xe one. This is due to the fact that the masses of Ar and He, which are, respectively, 66 and 6.6 yg, are much smaller than the mass of Xe. By comparing the results obtained in Figs. 7 and 8, it can be concluded that the proposed CNT-resonator can easily detect masses with few zepto-grams (10^{-21} g). Moreover, acceptable frequency shifts can be obtained with the proposed CNT for tens of yocto-gram (10^{-24} g) masses. However, for few yocto-grams, special considerations should be taken when designing mechanical resonators for these small sensitivities. Thus, with the aid of CNTs with smaller sizes and by adjusting the vibrational mode of the resonator according to the mass location, higher sensitivities (few yocto-grams) can be obtained.

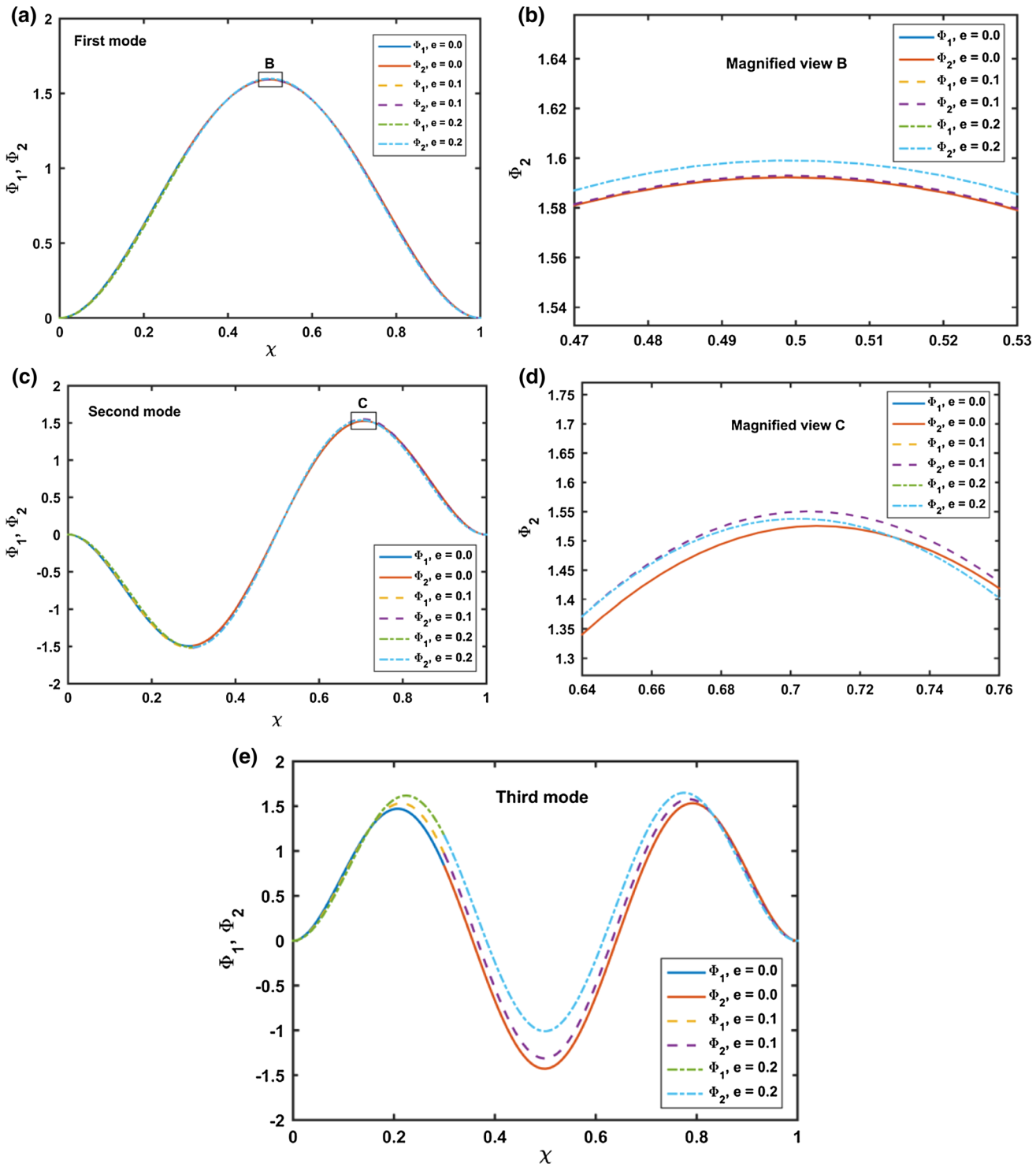

Fig. 5 Variations of the first three mode shapes of SWCNT when considering various values of the nonlocal parameter and when a single Xe-atom is deposited at $\eta = 0.3$

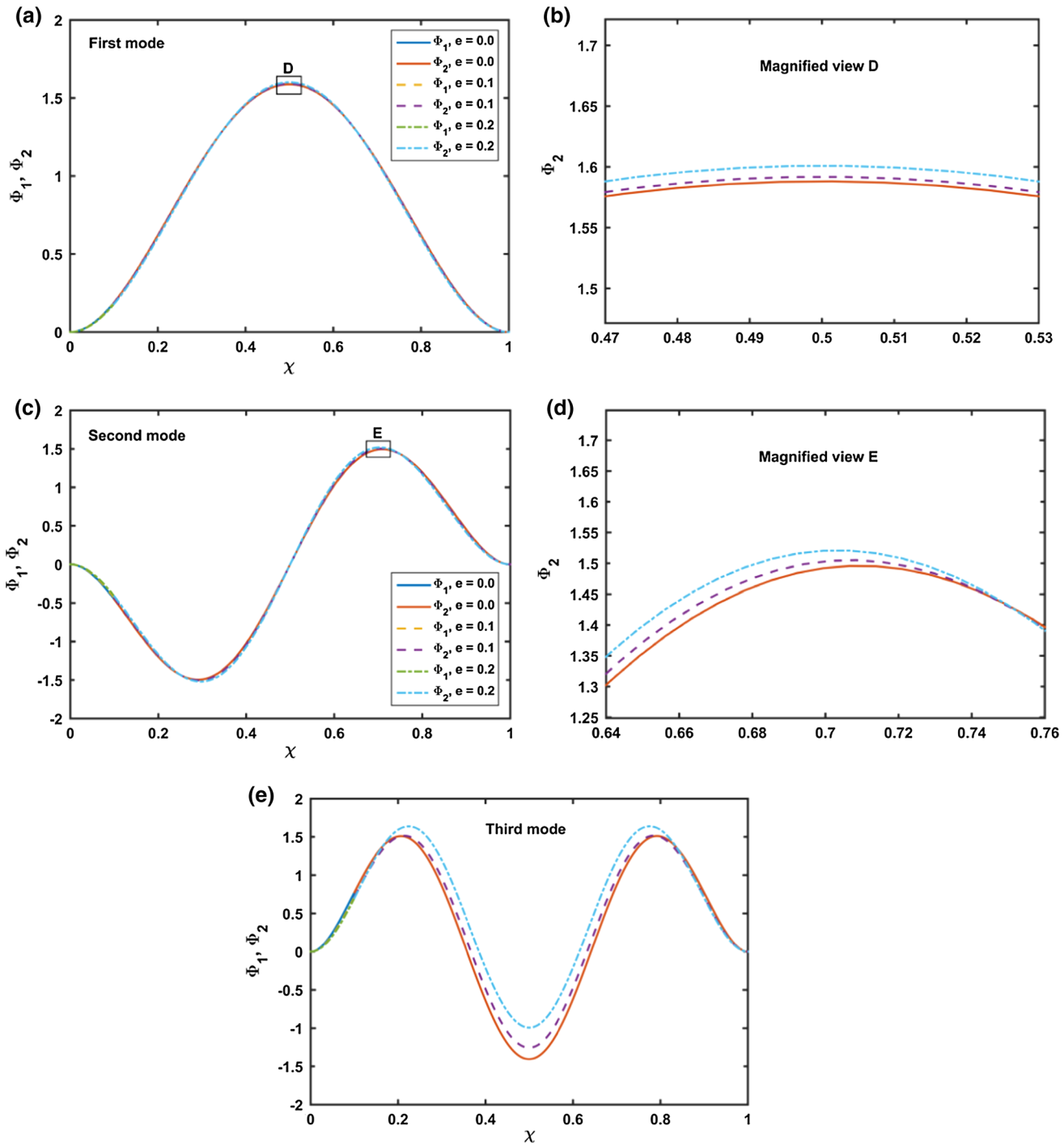

Fig. 6 Variations of the first three mode shapes of SWCNT when considering various values of the nonlocal parameter and when a single Xe-atom is deposited at $\eta = 0.1$

5 Conclusions

The nonlocal nonlinear equations of motion of bridged SWCNT-based mass nano-sensors have been derived based on the Euler–Bernoulli beam assumptions. An eigenvalue problem has been carried out in order to determine the effects of a deposited mass and its location on the natural frequencies and mode shapes of the SWCNT. A SWCNT-resonator was proposed to detect the mass of Xe, Ar, and He atoms. It was shown that the first three natural frequencies and mode shapes of the resonator are strongly dependent on the location of the deposited atomic-scale

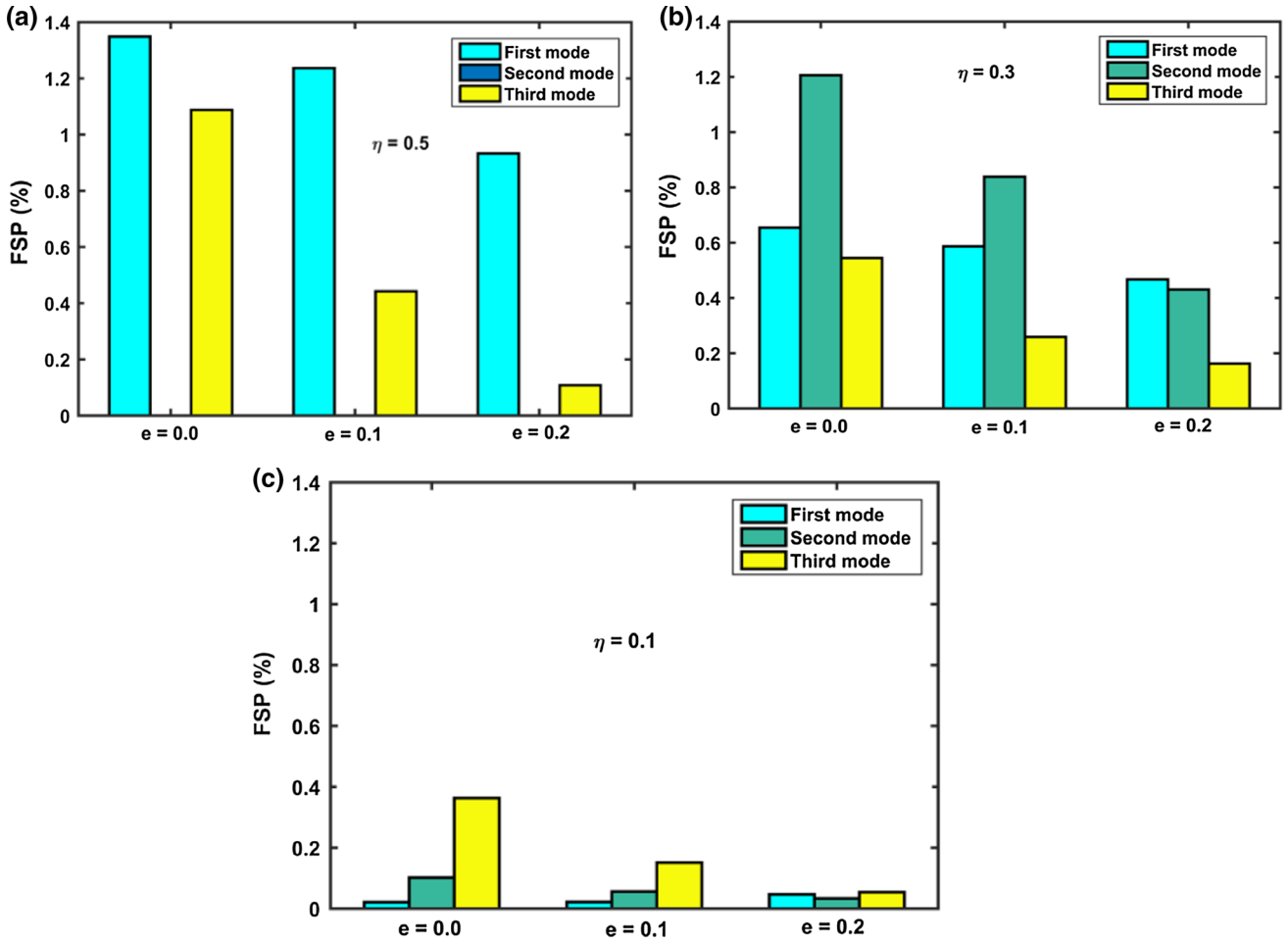

Fig. 7 Variations of FSP for the first three vibrational modes when varying the location of the deposited Xe-mass and the nonlocal parameter

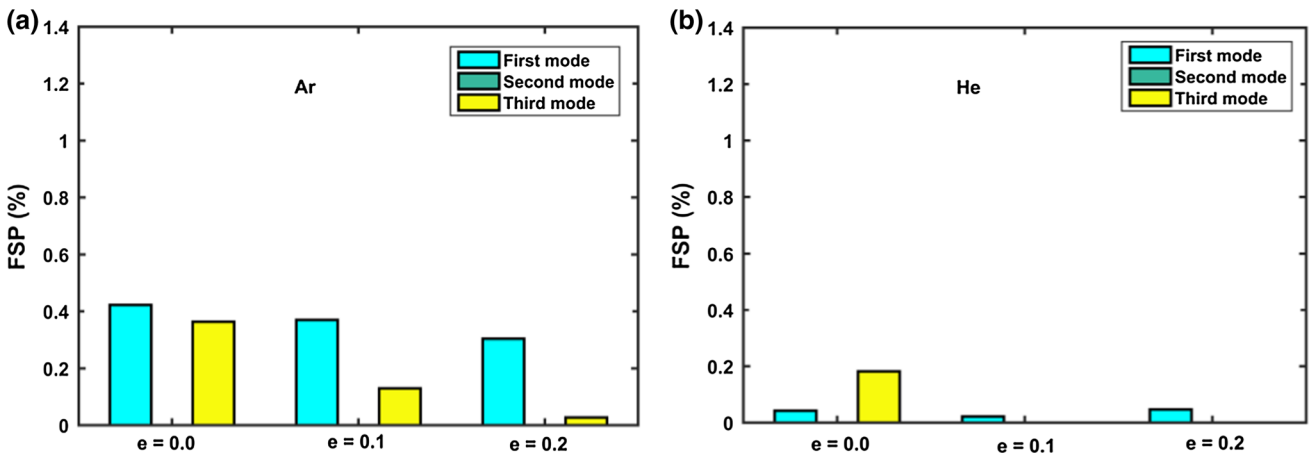

Fig. 8 Variations of FSP for the first three vibrational modes when considering **a** Ar and **b** He atoms and when the mass is located at $\eta = 0.5$

mass and the nonlocal nature of the CNT structure. It was proved that an increase in the nonlocal parameter is accompanied by a decrease in the natural frequencies of the mechanical resonator. According to the obtained results through this study, it can be concluded that the sensitivity of CNTs-resonators strongly depends on the location of the deposited mass. In addition, designing CNTs-resonators that can operate at different vibrational modes is beneficial

where the deposited mass can be located anywhere through the beam's length. Hence, to achieve higher sensitivities, the vibrational mode of the device can be adjusted according to the mass location. The obtained results also demonstrate that without knowing the exact location of the deposited particle, its estimated mass cannot be accurately determined.

References

1. Y. Tao, J.M. Boss, B.A. Moores, C.L. Degen, Single-crystal diamond nanomechanical resonators with quality factors exceeding one million. Nat. Commun. (2014). doi:10.1038/ncomms4638
2. A.K. Huttel, G.A. Steele, B. Witkamp, M. Poot, L.P. Kouwenhoven, H.S. van der Zant, Carbon nanotubes as ultrahigh quality factor mechanical resonators. Nano Lett. **9**, 2547–2552 (2009)
3. J. Moser, A. Eichler, J. Güttinger, M.I. Dykman, A. Bachtold, Nanotube mechanical resonators with quality factors of up to 5 million. Nat. Nanotechnol. **9**, 1007–1011 (2014)
4. M. Shaat, Effects of grain size and microstructure rigid rotations on the bending behavior of nanocrystalline material beams. Int. J. Mech. Sci. **94–95**, 27–35 (2015)
5. M. Shaat, A. Abdelkefi, Modeling of mechanical resonators used for nanocrystalline materials characterization and disease diagnosis of HIVs. Microsyst. Technol. **22**(2), 305–318 (2016)
6. M. Shaat, A. Abdelkefi, Pull-in instability of multi-phase nanocrystalline silicon beams under distributed electrostatic force. Int. J. Eng. Sci. **90**, 58–75 (2015)
7. M. Shaat, A. Abdelkefi, Modeling the material structure and couple stress effects of nanocrystalline silicon beams for pull-in and bio-mass sensing applications. Int. J. Mech. Sci. **101–102**, 280–291 (2015)
8. L. Sekaric et al., Nanomechanical resonant structures in nanocrystalline diamond. Appl. Phys. Lett. **81**, 4455–4457 (2002)
9. A.U. Hutchinson et al., Dissipation in nanocrystalline-diamond nanomechanical resonators. Appl. Phys. Lett. **84**, 972–974 (2004)
10. B. Lassagne, D. Garcia-Sanchez, A. Aguasca, A. Bachtold, Ultrasensitive mass sensing with a nanotube electromechanical resonator. Nano Lett. **4**(9), 1775–1779 (2008)
11. A. Dalgarno, W.D. Davison, Long-range interactions of alkali metals. Mol. Phys. **13**(5), 479–486 (1967)
12. R.J. Leroy, R.B. Bernstein, Dissociation energy and long-range potential of diatomic molecules from vibrational spacings of higher levels. J. Chem. Phys. **52**(8), 3869–3879 (1970)
13. V.M. Mostepanenko, I.Y. Sokolov, Hypothetical long-range interactions and restrictions on their parameters from force measurements. Phys. Rev. D **47**(7), 2882–2891 (1993)
14. P. Poncharal, Z.L. Wang, D. Ugarte, W.A. de Heer, Electrostatic deflections and electromechanical resonances of carbon nanotubes. Science **283**, 1513–1516 (1999)
15. C. Li, T. Chou, Mass detection using carbon nanotube-based nanomechanical resonators. Appl. Phys. Lett. **84**, 5246 (2004)
16. C. Li, T. Chou, Strain and pressure sensing using single-walled carbon nanotubes. Nanotechnology **15**, 1493–1496 (2004)
17. H. Chiu, P. Hung, H.W.C. Postma, M. Bockrath, Atomic-scale mass sensing using carbon nanotubes resonators. Nano Lett. **8**(12), 4342–4346 (2008)
18. S. Sawano, T. Arie, S. Akita, Carbon nanotube resonator in liquid. Nano Lett. **10**, 3395–3398 (2010)
19. Y. Wang, T.W. Yeow, A review of carbon nanotubes-based gas sensors. J. Sens. Article ID 493904, p. 24 (2009)
20. K. Balasubramanian, M. Burghard, Biosensors based on carbon nanotubes. Anal. Bioanal. Chem. **385**, 452–468 (2006)
21. C. Li, T.-W. Chou, Single-walled carbon nanotubes as ultrahigh frequency nanomechanical resonators. Phys. Rev. B **68**, 073405-3 (2003)
22. X.L. Feng, R. He, P. Yang, M.L. Roukes, Very high frequency silicon nanowire electromechanical resonators. Nano Lett. **7**(7), 1953–1959 (2007)
23. T. Murmu, M.A. McCarthy, S. Adhikari, Nonlocal elasticity based magnetic field affected vibration response of double single-walled carbon nanotube systems. J. Appl. Phys. **111**, 113511 (2012)
24. J. Li, K. Zhu, Weighing a single atom using a coupled plasmon-carbon nanotube system. Sci. Technol. Adv. Mater. **13**, 025006 (2012). **(6pp)**
25. R. Chowdhury, S. Adhikari, J. Mitchell, Vibrating carbon nanotube based bio-sensors. Phys. E **42**, 104–109 (2009)
26. S. Adhikari, R. Chowdhury, The calibration of carbon nanotube based bionanosensors. J. Appl. Phys. **107**, 124322 (2010)
27. I. Mehdipour, A. Barari, G. Domairry, Application of a cantilevered SWCNT with mass at the tip as a nanomechanical sensor. Comput. Mater. Sci. **50**, 1830–1833 (2011)
28. I. Mehdipour, A. Barari, Why the center-point of bridged carbon nanotube length is the most mass sensitive location for mass attachment? Comput. Mater. Sci. **55**, 136–141 (2012)
29. Y. Joshi, A. Hrasha, C. Shatma, Vibration signature analysis of single walled carbon nanotube based nanomechanical sensors. Phys. E **42**, 2115–2123 (2010)
30. T. Natsuki, N. Matsuyama, J. Shi, Q. Ni, Vibration analysis of nanomechanical mass sensor using carbon nanotubes under axial tensile loads. Appl. Phys. A **116**, 1001–1007 (2014)
31. H. Lee, J. Hsu, W. Chang, Frequency shift of carbon-nanotube-based mass sensor using nonlocal elasticity theory. Nanoscale Res. Lett. **5**, 1774–1778 (2010)
32. T. Murmu, S. Adhikari, Nonlocal frequency analysis of nanoscale biosensors. Sens. Actuators A **137**, 41–48 (2012)
33. M. Aydogdu, S. Filiz, Modeling carbon nanotube-based mass sensors using axial vibration and nonlocal elasticity. Phys. E **43**, 1229–1234 (2011)
34. Z. Shen, G. Tang, L. Zhang, X. Li, Vibration of double-walled carbon nanotube based nanomechanical sensor with initial axial stress. Comput. Mater. Sci. **58**, 51–58 (2012)
35. Z. Shen, X. Li, L. Sheng, G. Tang, Nonlocal Timoshenko beam theory for vibration of carbon nanotube-based biosensor. Phys. E **44**, 1169–1175 (2012)
36. K. Kiani, H. Ghaffari, B. Mehri, Application of elastically supported single-walled carbon nanotubes for sensing arbitrarily attached nano-objects. Curr. Appl. Phys. **13**, 107–120 (2013)
37. X. Li, G. Tang, Z. Shen, K. Lee, Resonance frequency and mass identification of zeptogram-scale nanosensor based on the nonlocal beam theory. Ultrasonics **55**, 75–84 (2015)
38. A.C. Eringen, *Nonlocal Continuum Field Theories* (Springer, New York, 2002)
39. A.C. Eringen, On differential equations of nonlocal elasticity and solutions of screw dislocation and surface waves. J. Appl. Phys. **54**, 4703 (1983)
40. C. Polizzotto, Nonlocal elasticity and related variational principles. Int. J. Solids Struct. **38**(42), 7359–7380 (2001)
41. X. Zeng, Y. Chen, J.D. Lee, Determining material constants in nonlocal micromorphic theory through phonon dispersion relations. Int. J. Eng. Sci. **44**, 1334–1345 (2006)
42. J. Peddieson, G.R. Buchanan, R.P. McNitt, Application of nonlocal continuum models to nanotechnology. Int. J. Eng. Sci. **41**, 305–312 (2003)

43. L.J. Sudak, Column buckling of multiwalled carbon nanotubes using nonlocal continuum mechanics. J. Appl. Phys. **94**, 7281–7287 (2003)
44. L.F. Wang, H.Y. Hu, Flexural wave propagation in single-walled carbon nanotubes. Phys. Rev. B **71**, 195412 (2005)
45. Y.Q. Zhang, G.R. Liu, X.Y. Xie, Free transverse vibrations of double-walled carbon nanotubes using a theory of nonlocal elasticity. Phys. Rev. B **71**, 195404 (2005)
46. P. Lu, H.P. Lee, C. Lu, P.Q. Zhang, Dynamic properties of flexural beams using a nonlocal elasticity model. J. Appl. Phys. **99**, 073510 (2006)
47. M. Xu, Free transverse vibrations of nano-to-micron scale beams. Proc. Roy. Soc. A **462**, 2977–2995 (2006)
48. J.N. Reddy, Nonlocal theories for bending, buckling and vibration of beams. Int. J. Eng. Sci. **45**, 288–307 (2007)
49. M. Shaat, Iterative nonlocal elasticity for Kirchhoff plates. Int. J. Mech. Sci. **90**, 162–170 (2015)
50. P. Lu, P.Q. Zhang, H.P. Lee, C.M. Wang, J.N. Reddy, Non-local elastic plate theories. Proc. R. Soc. A **463**, 3225–3240 (2007)
51. Y. Aboelkassem, A.H. Nayfeh, M. Ghommem, Bio-mass sensor using an electrostatically actuated microcantilever in a vacuum microchannel. Microsyst. Technol. **16**, 1749–1755 (2010)
52. S.A. Emam, A Theoretical and Experimental Study of Nonlinear Dynamics of Buckled Beams. PhD dissertation, (Virginia Polytechnic Institute and State University, Blacksburg, VA, 2002)
53. H.L. Dai, L. Wang, A. Abdelkefi, Q. Ni, On nonlinear behavior and buckling of fluid-transporting nanotubes. Int. J. Eng. Sci. **87**, 13–22 (2015)
54. T. Murmu, S. Adhikari, Nonlocal vibration of carbon nanotubes with attached buckyballs at tip. Mech. Res. Commun. **38**, 62–67 (2011)